# The SWAT Wavefront Sensor

Herbert T. Barclay, Phillip H. Malyak, William H. McGonagle, Robert K. Reich, Gregory S. Rowe, and Jonathan C. Twichell

**■ A team of researchers at Lincoln Laboratory built an advanced 241-channel Hartmann wavefront sensor for the adaptive optics system that was used in the Short-Wavelength Adaptive Techniques (SWAT) experiments. This sensor measures the phase of either pulsed or continuous sources of visible light. The instrument uses binary optics lens arrays made at Lincoln Laboratory to generate 16 × 16 subaperture focal spots whose centroids are measured with custom-built 64 × 64-pixel charge-coupled-device (CCD) cameras. The back-illuminated CCD detectors have quantum efficiencies of 85% at 500 nm; the camera has a readout noise of 25 electrons rms at 7000 frames/sec. A special pipeline processor converts the CCD camera data to wavefront gradients in 1.4 $\mu$sec. The sensor has an accuracy of $\lambda/15$ at an input light level of 2000 photons per subaperture.**

One of the key components of an adaptive optics system is the wavefront sensor [1]. Its function is to measure the phase of radiation from a beacon that has entered a telescope after probing atmospheric aberrations existing in the optical path of interest. These aberrations can be caused by turbulence and, for high-average-power laser beams, thermal blooming [2]. Measurements made by the wavefront sensor are used to control a deformable mirror, which leads to compensation either of a propagating laser beam or an image, depending on the application. Figure 1 shows a diagram of a typical adaptive optics system.

Rather than measuring phase directly, most wavefront sensors currently used in adaptive optics systems measure the two-dimensional gradients (i.e., the local wavefront tilts) at a discrete number of points in the pupil plane. The gradient data can then be reconstructed [3] either by digital [4] or analog [1] techniques into a least-squares approximation of the incoming wavefront. Signals based on the reconstructed phase are used to drive the actuators of the deformable mirror, thereby placing a figure proportional to the conjugate of the measured phase on its surface. Overall tilt is removed by the fast-steering mirror, thus minimizing requirements for both the gradient-measurement range of the sensor and the stroke of the deformable-mirror actuators.

We built a wavefront sensor as part of a 241-channel adaptive optics system used by Lincoln Laboratory in the recently completed Short-Wavelength Adaptive Techniques (SWAT) program. The field experiments in this program demonstrated the effectiveness of adaptive optics for turbulence compensation at visible wavelengths [5–7]. In particular, the experiments involved compensating an outgoing continuous-wave green argon-ion laser beam at 514 nm for atmospheric turbulence. The laser beam was propagated from a 60-cm beam director at the Air Force Maui Optical Station (AMOS) atop Mount Haleakala on the island of Maui.

The experiment called for real-time compensation of turbulence to produce a flat phase on the laser wavefront at the top of the atmosphere. The degree of compensation in the SWAT experiment was measured by pointing the laser beam at an array of detectors located on the Low-Power Compensation-Experiment (LACE) satellite [6]. This satellite, at a nominal altitude

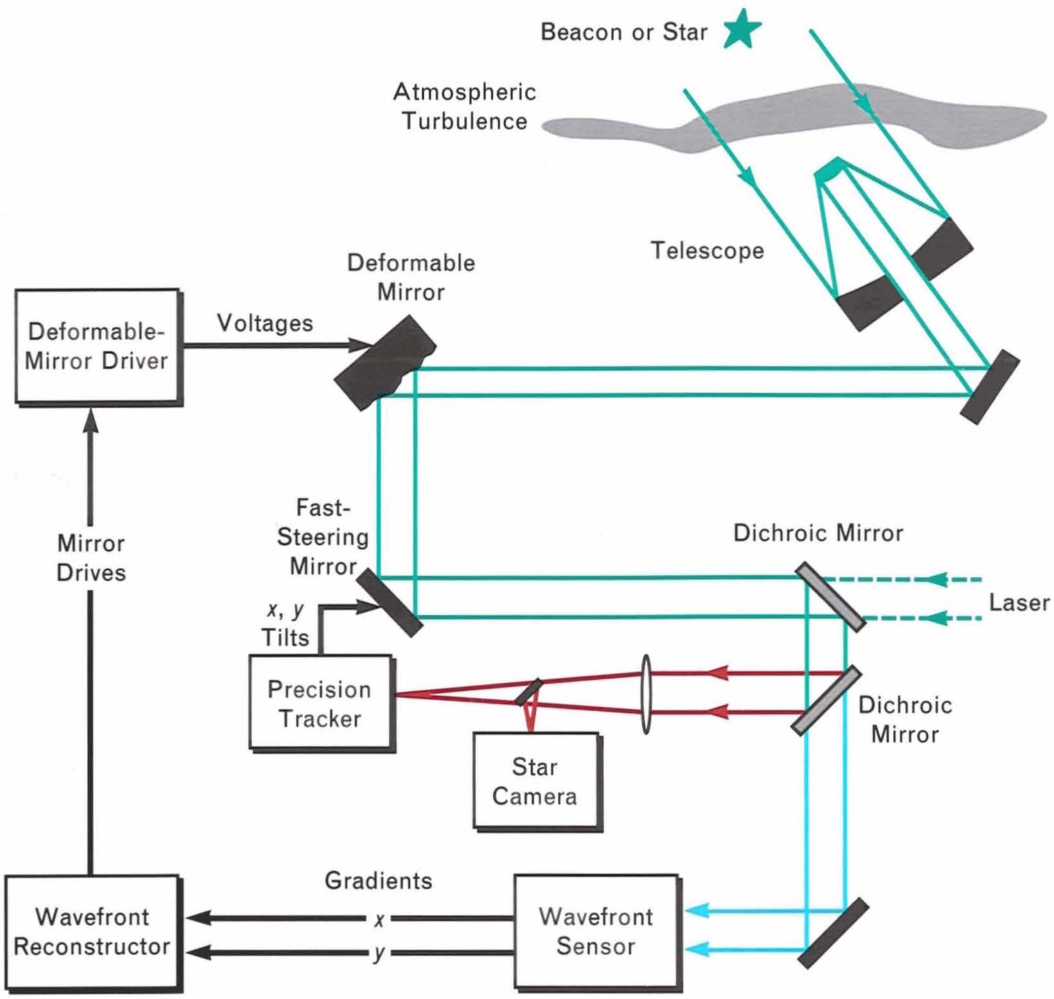


**FIGURE 1.** An adaptive optics system. Radiation from a beacon or star above the turbulence enters the telescope, reflects from the deformable mirror, and goes into the wavefront sensor, which measures the gradients of the wavefront. The reconstructed phase is used to control the surface of the deformable mirror. In the null-seeking mode of operation the mirror is deformed until the sensor measures a flat wavefront, at which time the mirror figure corresponds to the conjugate of the turbulence-aberrated beacon wavefront. The fast-steering mirror and precision tracker remove turbulence-induced tilt. If a laser beam is propagated in the opposite direction (outward), it will be precorrected for the instantaneous aberrations in the atmosphere.

of 500 km, also carries an array of retroreflectors that served as a reference beacon when illuminated from AMOS by a second laser, a continuous-wave blue laser at 488 nm.

In another mode of operation, instead of a retroreflector for the beacon, we used Rayleigh backscatter (generated by focusing a 508-nm pulsed dye-laser beam in the atmosphere at a range of 6 to 8 km) to sense the turbulence-induced wavefront errors [5, 7]. The Rayleigh backscatter produces a *synthetic* beacon. The pulse length of the dye laser was 1.8 $\mu$sec, the pulse energy transmitted was approximately 1 J, and the laser repetition rate was 5 Hz. The outgoing laser light was polarized; this polarization was retained by the backscattered light.

With a continuous-wave beacon, a null-seeking servo system can be used to achieve compensation. At the low repetition rates of the dye laser, however, the atmosphere changes significantly between pulses; compensation must therefore be based on the return from a single pulse. Operation of the adaptive optics system with low-repetition-rate pulsed beacons requires that the beacon wavefront be accurately determined on each pulse and that the deformable mirror quickly and accurately assume the shape to which it is commanded.

Operating the adaptive optics system in a pulsed, or *go-to,* mode leads to several system requirements beyond those needed for continuous-wave operation. The principal new requirement is the need for each of the adaptive optics components to be absolutely and accurately calibrated. The wavefront sensor must be calibrated so that its gradient outputs can be used by the reconstructor to generate calibrated signals for driving the deformable mirror. Additional sensor requirements on light input level, integration time, and tilt range also influence the measurement accuracy.

In this article we describe the wavefront sensor that we built for the SWAT experiments, and we present its measured performance. In addition to the wavefront sensor, the SWAT adaptive optics system included a 241-actuator deformable mirror, a digital reconstructor, and a tilt-compensation system. These components are described in more detail in the article by Daniel V. Murphy in this issue [6].

## Wavefront Sensors for Pulsed Operation

Adaptive optics systems use several types of wavefront sensors. One well-known approach, the rotating-grating shearing interferometer [8], has been used successfully in atmospheric-compensation experiments with a continuous-wave beacon source [2]. The duration of the synthetic beacon (approximately 10 $\mu$sec) in the SWAT experiments was too short, however, to be sampled by a rotating-grating instrument (whose typical sampling interval is greater than 20 $\mu$sec). This approach was therefore inappropriate for our pulsed applications.

The sensor that we built is based on the Hartmann principle of wavefront testing that is well known in the optics community. This type of sensor has no moving parts and is therefore well suited to pulsed operation. Figure 2 illustrates the principle of the

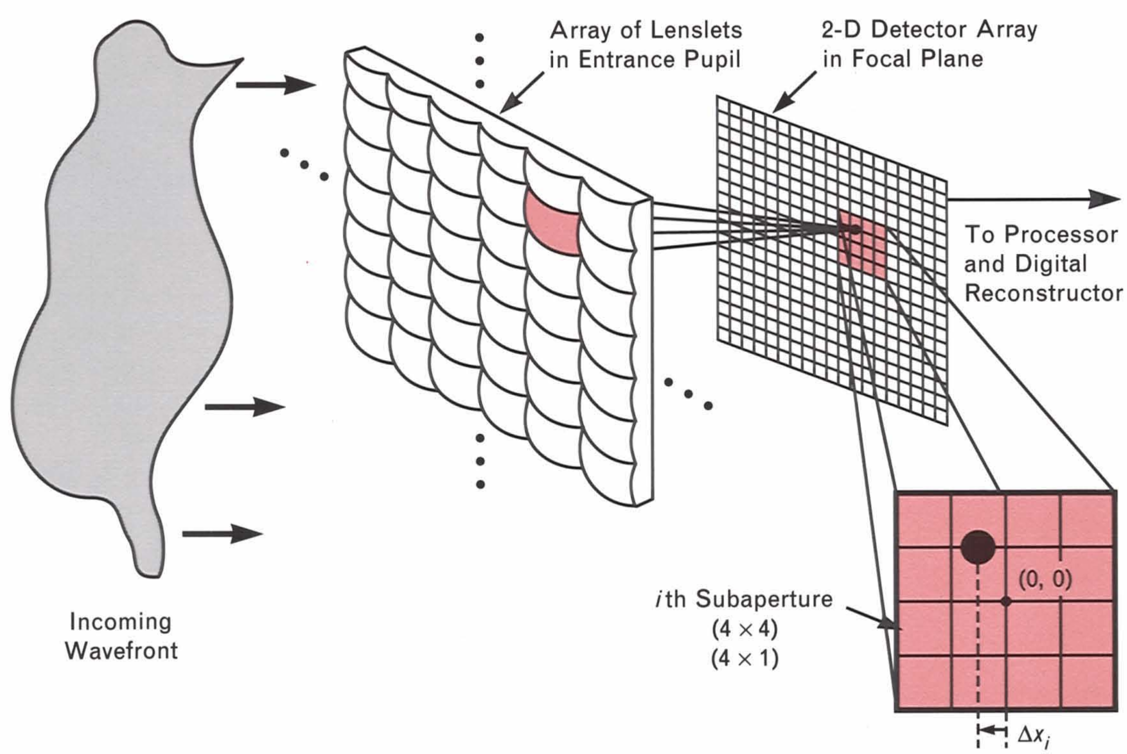


**FIGURE 2.** Operating principle of the Hartmann sensor. The local phase gradient at a subaperture is proportional to the centroid of the focal spot formed by the corresponding lenslet. Each subaperture in the Short-Wavelength Adaptive Techniques (SWAT) sensor is mapped into a 4 x 4-pixel array.

Hartmann sensor. The input pupil is segregated into subapertures by an array of small lenses. Each lenslet focuses the light it receives into a tight spot on the detector plane, where its position can be measured.

The Hartmann scheme represented in Figure 2 shows a subaperture focal spot falling on a 4 × 4-pixel area of a larger detector array. The instantaneous phase gradient at that subaperture is proportional to the position of the centroid of the focal spot. In practice, we divide the light from the input pupil into two beams of roughly equal intensity, and use two sets of lens arrays and cameras to measure gradients in the $x$ and $y$ directions, respectively.

The wavefront measurement approach assumes that the subaperture size $a$ is sufficiently small so that no significant aberration of order higher than tilt exists on the wavefront over any subaperture. The focal-spot intensity distribution is then diffraction limited and, for a square subaperture, is given by

$$I_s(x, y) = I_0 \operatorname{sinc}^2\left(\frac{a(x - x_0)}{f\lambda}\right)\operatorname{sinc}^2\left(\frac{a(y - y_0)}{f\lambda}\right),$$

where $I_0$ is the peak intensity, $f$ is the focal length, $\lambda$ is the wavelength, $x_0/f\lambda$ is the $x$ tilt in waves, and $y_0/f\lambda$ is the $y$ tilt in waves. The width $w$ of the main lobe is

$$w = \frac{2f\lambda}{a}.$$

Specific sensor requirements determine the choice of values for the subaperture size $a$ and the focal length $f$.

## Sensor Requirements for SWAT

The specific characteristics of the atmospheric turbulence to be compensated determine the spatial and temporal requirements for the adaptive optics system and, in particular, for the sensor. For a given optical aperture $D$, the approximate number of adaptive channels needed is given by $(D/r_0)^2$, where $r_0$ is the Fried turbulence coherence length [9]. The coherence length $r_0$, which is a measure of the strength of turbulence, varies from site to site and depends on wavelength $\lambda$ and zenith angle $\theta$:

$$r_0 \propto \lambda^{6/5} \cos\theta .$$

The coherence length $r_0$ at the AMOS site was typically 5 to 10 cm at visible wavelengths and small zenith angles, and as small as 3 to 4 cm at larger angles from zenith. For the SWAT system, when used with the 60-cm AMOS beam director, a subaperture dimension of 3.75 cm was chosen (referred to the telescope output pupil plane), which corresponded to a value of 16 for $D/r_0$ (i.e., 16 actuators across the 60-cm diameter).

The time available for measuring the atmospheric path and placing the appropriate figure on the deformable mirror depends on the time over which the turbulence along the path remains essentially constant. For the SWAT experiments, this time was limited by the relatively large angular slew rate (approximately 1 deg/sec) of the LACE satellite. To maximize the performance of the adaptive optics system, the entire compensation process—from measuring the gradients to reconstructing the phase to actuating the deformable mirror—had to take place in a fraction of a millisecond. These spatial and temporal requirements on the adaptive optics system also have implications for other system performance parameters, including measurement accuracy (particularly at low light levels), tilt range, and update rate. These implications are described in the following sections.

### *Measurement Accuracy*

Contributions from several error sources determine the quality of compensation that can be achieved with adaptive optics [7]. The error criterion for gradient measurements was chosen to be consistent with other known limitations in the system (i.e., neither so large that it dominated other errors nor so small that it added unreasonable technical demands). The accuracy requirement was set at $\lambda/15$ rms, for both closed-loop and go-to modes of operation.

For measuring phase gradients with a given accuracy, a certain number of photons must be counted during the measurement time [8]. In practice, a small number of photons reach the sensor from a synthetic beacon. For the SWAT system, which was required to perform good compensation at visible wavelengths, beacon photons were particularly precious because of the relatively small subaperture area, short measurement time, and small cross section for Rayleigh backscatter.

The SWAT sensor was required to meet the specified $\lambda/15$ accuracy with only 2000 input photons per subaperture for each channel ($x$ and $y$). The origin of this requirement is partly historical. At the time the sensor was being designed, the best quantum efficiency possible with an image intensifier was approximately 12%. Thus the 2000 photons would generate 240 photoelectrons. Assuming that the rest of the system was noiseless, this number of photoelectrons would yield $\lambda/15$ accuracy [10]. Thus 2000 photons per subaperture was considered a suitable goal for the specification.

### *Tilt Range for Gradient Measurements and Linearity*

In closed-loop operation, the wavefront sensor needs to be accurate only near the null position for each subaperture. Once the wavefront sensor captures the beacon image and compensation is initiated, only small departures from null occur and linearity is not a serious concern. In the go-to mode, on the other hand, the sensor must measure the wavefront to an accuracy of $\lambda/15$ by using a single beacon return. For any given return the full range of aberrations (apart from overall tilt) originating in the atmosphere, in the telescope dome, and from elements such as lenses and mirrors in the optical train, can appear on the wavefront at the sensor. (Overall tilt is removed by a separate precision tracker and fast-steering mirror). We estimated that the peak-to-peak wavefront excursions seen by the sensor at AMOS would be as large as ±1.1 waves per subaperture.

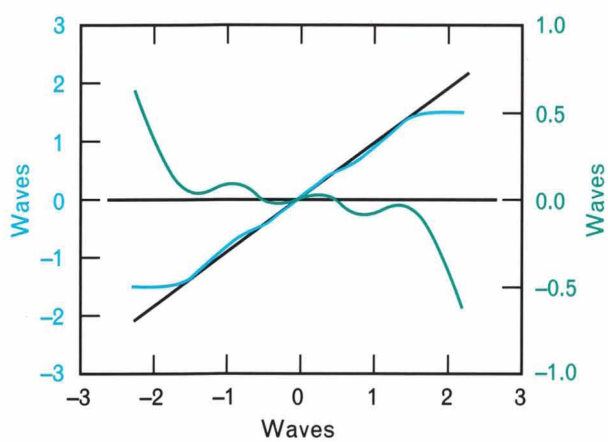


**FIGURE 3.** Calculated transfer curve for a 72.5-mm focal-length 400-$\mu$m square lenslet. This curve characterizes an ideal single subaperture with no light from neighboring subapertures contaminating the measurement. The figure shows the ideal unity-slope response, the calculated response for the actual SWAT lenslet, and the difference between them.

The requirement that energy from the focal spot in one subaperture should not spill over into another subaperture limits the phase gradient that can be measured by a Hartmann sensor. Selection of the optimum spot size (and thus the optimum focal length) involves a trade-off between the linearity and the range of the tilt measurement. This trade-off is most easily examined in terms of the resulting *transfer curve*, which is a plot of the measured tilt versus the actual input wavefront tilt for a single subaperture. Figure 3 shows an ideal transfer curve as well as the calculated transfer curve for the lens arrays used in the SWAT system.

An ideal sensor has a transfer curve that is a perfect straight line through the origin, with a slope of unity. In practice, because a small number of pixels ($4 \times 4$) are used to calculate the centroid, the transfer curve shows structure related to the pixel structure. For the SWAT sensor we required the slope of the transfer curve to vary by less than ±15% to provide good servo stability in closed-loop operation. This restriction established the focal length of the lenslets (greater than 72.5 mm) and the focal spot size (at least 1.8 pixels).

The limit to the tilt range arises from the measurement error associated with energy from one focal spot spilling into an adjacent subaperture. We arbitrarily selected a limit of $\lambda/10$ for the spillover error. With the minimum spot size allowed by linearity constraints, the maximum acceptable tilt range was ±1.6 waves.

### *System Update Rate*

An important requirement of the SWAT experiments was that the system be able to make corrections by using pulsed backscatter returns from multiple beacon lasers that are transmitted sequentially in time. Data from these returns are then stitched together to provide improved accuracy in wavefront compensation [7, 11, 12]. Because we were prepared to use as many as five separate beacons, we required the wavefront measurement to be made in 125 $\mu$sec (i.e., gradients from each beacon are measured and sent to the reconstructor within 125 $\mu$sec). This measurement cycle left adequate time for the deformable mirror to respond and settle to its commanded figure.

## SWAT Wavefront Sensor

The Hartmann sensor used for the SWAT program incorporates three key features that enabled it to meet the above requirements. The first of these features is the binary optics lenslet array (made at Lincoln Laboratory) that was used to produce the subaperture focal spots. The second feature is the CCD focal-plane detector array and camera (also built at Lincoln Laboratory) that was used to measure the focal-spot centroids. The third feature is the unique approach that was taken to process the gradient signals.

### *Binary Optics Lenslet Array*

Because the sensor needs all the photons it can get from a beacon, the optics that produce subaperture focal spots must collect the light efficiently. Scattering and transmission losses must be minimized, of course, but a large fill factor is equally important. Each lens should have the same focal length and wedge angle, and the fill factor should approach 100%. The specific individual lenses needed for the SWAT sensor are 0.4 × 0.4 mm square, with 72.5-mm focal lengths.

The lens arrays in the Hartmann sensor were made at Lincoln Laboratory with a technique known as binary optics [13]. Binary optics uses plasma etching methods developed for VLSI integrated circuit fabrication to approximate closely a Fresnel lens. The maximum etch depth required for any lens is one wave of optical-path length, as shown in Figure 4. The quality of the resulting lens depends on how closely the surface approximates the correct shape. This shape is described numerically by the diffraction efficiency, which is the fraction of light passing through the lens

| Diffraction Efficiency | Number of Phase Levels | Number of Masks |
|---|---|---|
| 41% | 2 | 1 |
| 81% | 4 | 2 |
| 95% | 8 | 3 |
| 99% | 16 | 4 |
| 100% | $2^N$ | $N$ |

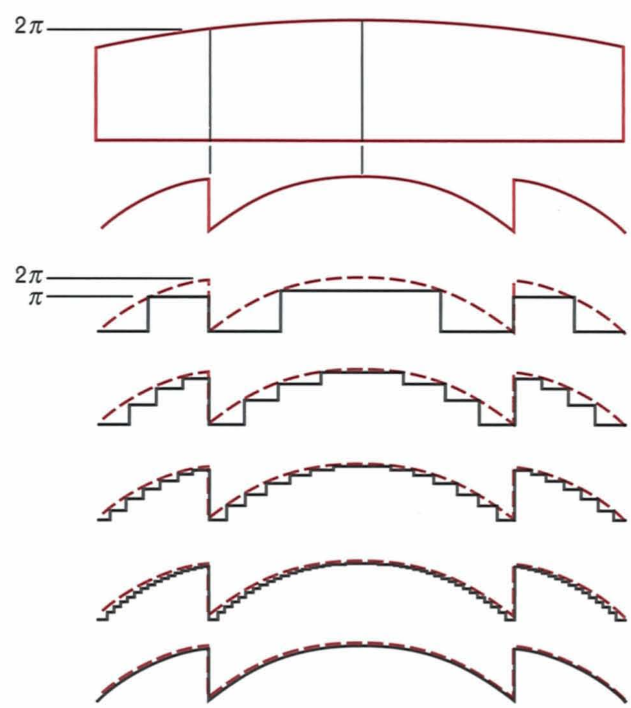


**FIGURE 4.** Binary optics diffraction efficiency. The shape of a Fresnel lens can be closely approximated by using binary optics techniques. The SWAT lens array was prepared with five masks, which yielded a theoretical diffraction efficiency of 99.7%.

that is properly diffracted into the focal spot.

The 16 × 16 array of binary optics lenses in the SWAT sensor form a 6.4 × 6.4-mm square. This size was chosen to be compatible with the beam-reducing telescope in the sensor. Each lens touches its neighbors without gaps, which produces a 100% fill factor that matches the lens array to the format of the CCD camera. The 16 × 16 array is part of a 1-in-diameter piece that is covered with lenses. Five masks were used in the fabrication process; the ideal shape of the lenses is thus approximated by $2^5$, or 32, steps, so the diffraction efficiency is greater than 99%. These lens arrays are highly uniform in focal length and spacing.

### *CCD Focal-Plane Arrays and Cameras*

As was pointed out earlier, accurate centroid measurements require optimum use of the arriving photons (i.e., good quantum efficiency) and low detector-associated noise. For the Hartmann detector two options were possible. The first option was to use a bare (i.e., unintensified) CCD focal-plane array with high quantum efficiency and low readout noise. The second option was to use an image intensifier, which would avoid the readout noise of a focal-plane array. In principle the intensified detector provides the advantage of noiseless front-end optical gain, but experience in the early phases of sensor development taught us that the intensified devices had several problems, including thermally induced mechanical drift, significant scattering within fiber optic couplings, poor quantum efficiency, and susceptibility to damage.

For many years an ongoing development program at Lincoln Laboratory has advanced the state of the art in CCDs [14]. In the early stages of the SWAT program, we anticipated that CCDs could be fabricated with a quantum efficiency of 85% at the SWAT operating wavelengths (488 to 508 nm), and with camera system noise less than 30 noise electrons, at readout rates of 5 Mpixels/sec in each of two parallel readout ports. This performance, incidentally, far exceeded any that could be obtained from commercial CCD vendors.

Analysis comparing bare and intensified CCDs as detectors for a Hartmann sensor showed that with the above characteristics the bare CCDs would perform as well as or better than the intensified devices, and would meet the SWAT requirements. Consequently, we decided to use bare CCDs, and a pair of arrays was designed and built at Lincoln Laboratory. Each array has 64 × 64 pixels, and each pixel is 27 $\mu$m on a side with 100% fill factor, which provides 4 × 4 pixels per subaperture.

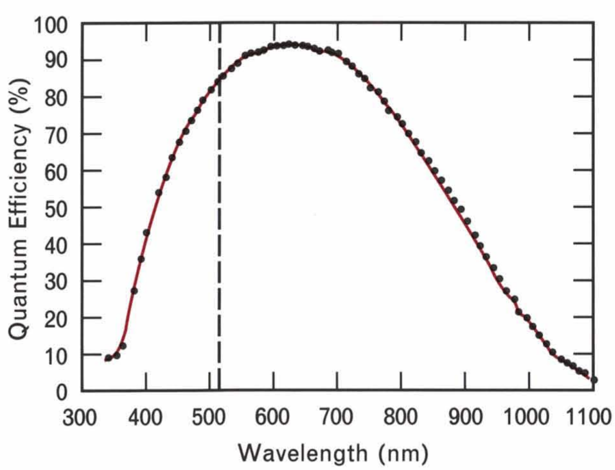


**FIGURE 5.** Measured quantum efficiency of the back-illuminated CCD focal planes used in the sensor. The arrays are antireflection coated with silicon monoxide for optimum performance near 500 nm.

Figure 5 shows the quantum efficiency achieved by the improved CCD devices. Illuminating the devices from the back circumvents the problem of the incident light having to penetrate the CCD circuitry (which is somewhat opaque to blue light). The devices were thinned to approximately 10 $\mu$m for back-illuminated operation [15]. In addition, a quarter-wave antireflection coating of silicon monoxide was applied to maximize the coupling of photons into the silicon.

The CCD cameras have a measured noise of 20 to 25 electrons root mean square (rms) at a readout rate of 5 Mpixels/sec. To achieve this low noise at such high readout rates, a two-stage source-follower located on the CCD chip does the charge-to-voltage conversion. The sense field-effect transistor is optimized for low gate capacitance and high responsivity. The temperature of the device is actively stabilized at 14 to 15°C with a Peltier-effect cooler to keep the amplifier gain stable and to minimize dark-current variations with temperature. The dark current of the silicon is less than 1 $nA/cm^2$ (less than 45 electrons per pixel per msec); it contributes less than 10% of the total noise variance.

The SWAT device uses a frame-transfer architecture with three phase clocks; Figure 6 shows the architecture of the device. Pixel charges in the 64 × 64 photon-collecting array, or *staring* array, can be shifted either up or down. Upward shifting moves any charge (photon-generated or dark current) into a charge dump at the top of the array. Downward shifting slides the image charges into the bottom half of the chip, which is a 64 × 64 buffer-storage array covered with an aluminum light shield. This frame-transfer operation takes 12 μsec in either direction. In gated operation the array is first cleared by upward shifting; then the array is quiescent during the desired stare time. Finally, the array is shifted down into the storage frame.

While waiting to be transferred into the buffer-storage array, each row of pixels has a different exposure time to incoming light. When a synthetic beacon is used, a Pockels cell and two polarizers with an open time of 5 to 10 μsec are used to shutter the camera, thus preventing the image from being smeared. The array in the storage buffer is then read out a line at a time. The horizontal shift register at the bottom of the array has a charge-to-voltage amplifier at each end. The CCD device has two readout ports, each of which can operate at 5 Mpixels/sec.

The charge of four rows of pixels is summed in the horizontal shift register before being read out. This summation is easily done by vertically shifting the four rows of charge into the horizontal register before reading the register. This mode of operation, called *binning*, is inherently free of noise (except for the summing of dark current) because charge is summed before detection. Binning reduces the number of readout cycles from 4096 (64 × 64) to 1024 (16 × 64). Because the summing occurs one line at a time, 4-pixel binning increases the frame rate to over 7000 frames/sec. Although the sensor is normally operated

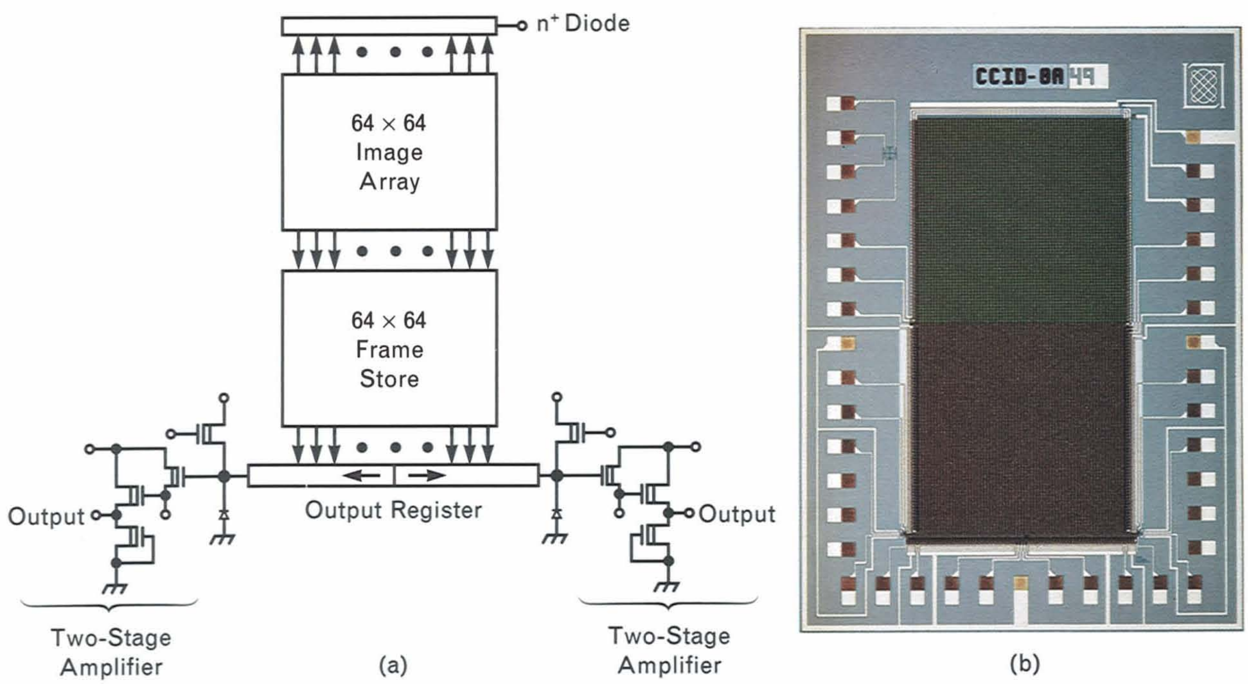


**FIGURE 6.** (a) Schematic diagram and (b) photograph of the two-port CCD used in the SWAT wavefront sensor. Photoelectrons collected in the image array can be shifted upward into a diode to clear the array of charge quickly. Shifting the photon-generated charge array downward into the frame-store array terminates the exposure of the frame by hiding the image under an aluminum light shield. Readout proceeds by shifting a line of charge into the output register and clocking the charge a pixel at a time into the two readout amplifiers.

in binned mode, the camera can also be run without binning; it is used in this manner when the focal spots are being aligned to the middle of the 4 × 4-pixel subaperture.

Lincoln Laboratory has made significant strides in CCD technology since the time the SWAT sensor was built. Cameras with four output ports and with 10-electron noise floors (compared to the 25-electron noise floor of the SWAT cameras) are now being built. The additional ports make higher data-rate operation possible even at lower light levels. Furthermore, on-chip electronic shuttering has been demonstrated with extinction ratios greater than 75,000 and shutter transition times less than 55 nsec [16]. An on-chip shutter with these capabilities eliminates the need for a Pockels cell with a SWAT-like sensor.

### *Wavefront Processor*

Each of the CCD cameras generates a 12-bit serial data stream of either 1024 or 4096 words, at a maximum rate of 11 Mwords/sec. The function of the wavefront processor is to convert the data from the cameras into gradients, which are then sent to the reconstructor. In addition, the processor directs intensity data generated at each subaperture to a real-time display and to a recording system.

A correction for offset and slope is performed on the raw intensity data for each pixel in the camera. The first step in the correction process is to subtract the background from the CCD camera data. This step removes any fixed pattern noise in the CCD and permits a dark condition to be recognized and represented by a value of zero. Next, the quantum efficiency is normalized with a gain correction. This normalization produces a value that accurately represents the incident light on each pixel. Thus, if $I_p$ is the corrected intensity value for pixel $p$, then

$$I_p = \left(C_p - O_p\right) G_p \,,$$

where $p$ is the pixel number (0 to 1023), $C_p$ is the camera value for pixel $p$, $O_p$ is the background offset for pixel $p$, and $G_p$ is the gain correction for pixel $p$ (in practice the CCDs are so uniform that the gain correction $G_p$ can be set to 1 for all pixels).

Next, the (one-dimensional) centroid of the focal spot for each pixel is calculated. This centroid is also called the *raw tilt* because it has yet to be converted into a wavefront tilt. Figures 2 and 7 illustrate how the processing that arrives at the raw tilt is carried out in binned 4-pixel groups. Let $s$ be the subaperture number (0 to 255) and let $I_{s,0}$, $I_{s,1}$, $I_{s,2}$, and $I_{s,3}$ be the 4-binned corrected intensity values for subaperture $s$. The raw tilt is then given by $R_s = N_s / D_s$, where

$$N_s = -3I_{s,0} - I_{s,1} + I_{s,2} + 3I_{s,3}$$

and

$$D_s = I_{s,0} + I_{s,1} + I_{s,2} + I_{s,3} \,.$$

$N_s$ is the sum of location-weighted intensities in the subaperture, and $D_s$ is the sum of the unweighted subaperture intensities. A low-light flag is set in the processor if the value of $D_s$ is less than 120 photons. The operator can choose to force the gradients that are sent to the reconstructor to be zero when a low-light flag is set.

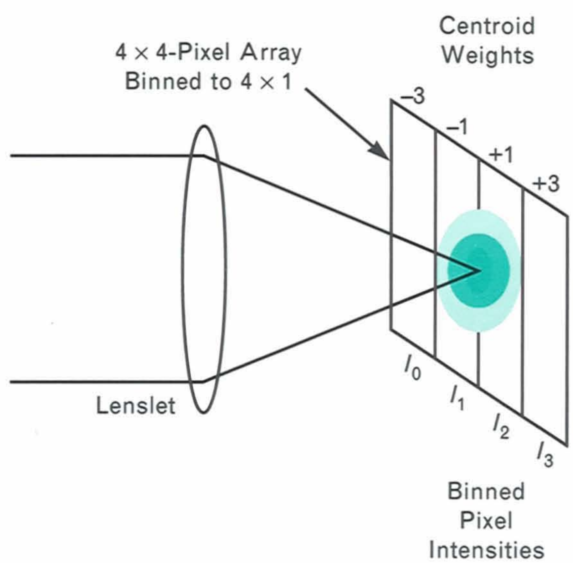


**FIGURE 7.** Nomenclature and weights for a single subaperture. The 4 × 4-pixel array for a single subaperture is binned to appear as a 4 × 1 array. Binning is accomplished by shifting four lines of charge at once into the output register for readout. For the case shown, the one-dimensional centroid of the focal spot along the horizontal axis is calculated by weighting the summed intensities in the vertically binned columns by their locations, relative to the center line.

The ratio of the two sums $N_s$ and $D_s$ is determined in two steps. First the inverse of the denominator $D_s$ is located in a lookup table in PROM; this table produces a 24-bit value. A 24-bit multiplier then multiplies that value by the numerator $N_s$. The result thus retains 12-bit intensity precision over the entire intensity dynamic range of the sensor. The calculated centroid, or raw tilt, is converted to the actual subaperture tilt, or gradient, through the *tilt gain*. The tilt gain is determined before an experiment begins by introducing a high-quality laser beam of precisely controlled tilt into the sensor and recording the measured raw tilt. A gain table calculated with the host VAX computer is then loaded into the memory of the wavefront processor. During an experiment the raw tilts are replaced in real time by the values in the tilt-gain table.

Before the gradients represent the correct figure to be placed on the deformable mirror, however, one additional step must be completed. This step is necessary to account for certain aberrations that are seen by the wavefront sensor but that must not be corrected on the deformable mirror. For example, as can be seen in Figure 1, aberrations in the optical path between the wavefront sensor and the dichroic mirror for the star camera are included in what the sensor measures, but because these aberrations are not in the path to the camera they won't affect the image. Therefore, these so-called *non-common-path* aberrations must not be included in the phase command to the deformable mirror. Fortunately, these aberrations are easily measured by injecting a flat wavefront into the non-common path and recording the resulting gradients. The last step in processing a wavefront, then, is to subtract the non-common-path contribution from the measured gradients. The resulting set of gradients is sent to the phase reconstructor.

The highly optimized wavefront processor, which is shown in Figure 8, comprises 1000 integrated circuits and occupies four 16-in-square circuit boards. A pipeline architecture is used to handle the two 10-Mword/sec data streams from the $x$ and $y$ CCDs. The pipeline stages correspond to the gradient-processing steps described above: CCD radiometric correction consisting of background subtraction and gain normalization, weighted and unweighted summation of numerator and denominator, high-precision division to generate raw tilt, and tilt correction consisting of tilt gain and offset. Because of our previous experience with wavefront sensors, we decided early in the

**FIGURE 8.** SWAT wavefront-sensor electronics. The upper portion of the sensor electronics rack contains the pipeline processor. Several diagnostics, including real-time readouts for average tilt and intensity, are visible on the front panel.

design stage to incorporate robust diagnostics. The data stream can be sampled at each of the major stages in the processor pipeline, which allows observation of the internal function of the processor. Data at these points can also be forced to a preset sequence of values, which allows definitive tests of proper functionality. A computer interface provides the path to load and read all the processing and diagnostic tables stored in the processor. This interface also provides both processor control functions and control of the automated functions in the sensor optical head (such as the calibration mirror).

The phase reconstructor is a massively parallel matrix multiplier [4]. It takes the set of 512 gradients (256 for the $x$-axis, 256 for the $y$-axis) as a column matrix and multiplies it by a $256 \times 512$ reconstruction matrix, which results in 256 phases. The matrix multiplication requires 262,144 arithmetic operations. The reconstructor performs this calculation with 512 parallel multiplier-accumulators in 55 $\mu$sec. An additional 50 $\mu$sec are required to transfer the reconstructed phase to the deformable mirror driver.

To operate the deformable mirror in the go-to mode, we designed the driver amplifiers to minimize the hysteresis and temperature dependence of the deformable mirror actuators. As a result, in a single step the entire surface of the mirror can go to its commanded position in less than 200 $\mu$sec with an accuracy of 0.02 $\mu$m rms ($\lambda/25$ at 500 nm).

## Wavefront-Sensor Layout

Figures 9 and 10 show a schematic diagram and a photograph, respectively, of the SWAT sensor optics. The sensor occupies a $3 \times 4$-ft area on the optical bench, and the sensor optics are enclosed in a light-tight box. External light enters through a shutter that can be closed during calibration procedures to isolate the sensor.

Fast shuttering during the frame-transfer time of the CCD cameras is accomplished with a pair of crossed polarizing beam splitters and a Pockels cell. The front beam splitter is also used to couple the beam from an internal tilt-calibration laser into the sensor optics. The calibration source is a small air-cooled argon-ion laser that provides a flat wavefront with adjustable tilt.

The pair of lenses used to image the deformable mirror on the wavefront-sensor input pupil reduces the beam size from the normal 16 mm at the entrance aperture of the sensor to 6.4 mm at the lens array. A phase plate and polarizing beam splitter divide the incoming light into two equal intensity beams, one for the $x$ camera and one for the $y$ camera. Each beam impinges a corresponding binary optic lens array that generates the Hartmann spots. The resulting focal-spot patterns are imaged by the CCD cameras.

## Calibration

The SWAT wavefront sensor has a robust calibration capability. Calibration involves several steps: alignment of the optics, CCD camera calibration, tilt gain calibration, and static aberration correction. Of these operations, the alignment of the sensor optics to the deformable mirror consumes the most time because it is done by hand. The rest of the calibration of the sensor is routine and has been automated with the aid of a VAX computer.

Each optical axis in the sensor has a commercial video camera to assist in the alignment of the Hartmann lens arrays to the deformable mirror. These cameras view the optical path via fold mirrors that can be dropped into place under remote control. Each camera is mounted on a slider assembly to permit viewing either the lens array or the focal spot array.

The CCD cameras must be aligned to the Hartmann lens arrays to within 1 $\mu$m. Each camera head is on a five-axis mount and can be precisely adjusted in translation along the two transverse axes, rotation about the optical axis, and distance from the lens array. Several real-time displays generated by the computer are used during the alignment operation. The computer can show the uncorrected and corrected camera data as pseudo-color images. Gradients, both raw and corrected, are displayed as an array of arrows. The gradient display also gives numeric values for the best estimates of the required camera movement to reduce the average gradient to zero.

Each CCD has a mechanical shutter that can be closed to record the fixed pattern noise. A radiometric calibration source consisting of an LED and a digitally controlled constant-current source can be swung into the beam path of each CCD to calibrate the pixel responsivity.

The tilt gain is calculated by generating the raw tilt transfer curve for each subaperture with a computer-controlled two-axis mirror. This mirror was built by Lincoln Laboratory and has a tilt noise of $\lambda/100$. The position sensors of the mirror are calibrated to $\lambda/30$ with an autocollimator and a set of interferometrically calibrated wedges.

## Performance

The sensor has achieved the goal of $\lambda/15$ performance with 2000 photons per subaperture. Measurements made to demonstrate this performance include CCD camera background noise, tilt transfer curves for each of the subapertures, and gradients as a function of input light level.

Figure 11 shows the measured transfer curves for all 256 of the subapertures of the $x$ camera. The rms deviation from linearity of the best fit to the measured transfer curve was $\lambda/28$ over a tilt range of $\pm 1.25$ waves. As was mentioned previously, pixel structure causes the small deviations from linearity of the transfer curves. Figure 12 compares the measured transfer curve of a subaperture to the ideal transfer curve. The expected tilt gain is 0.81; the measured value ranges from 0.70 to 0.75. The difference is primarily due to an intentional defocus of the lens array to increase the tilt range slightly.

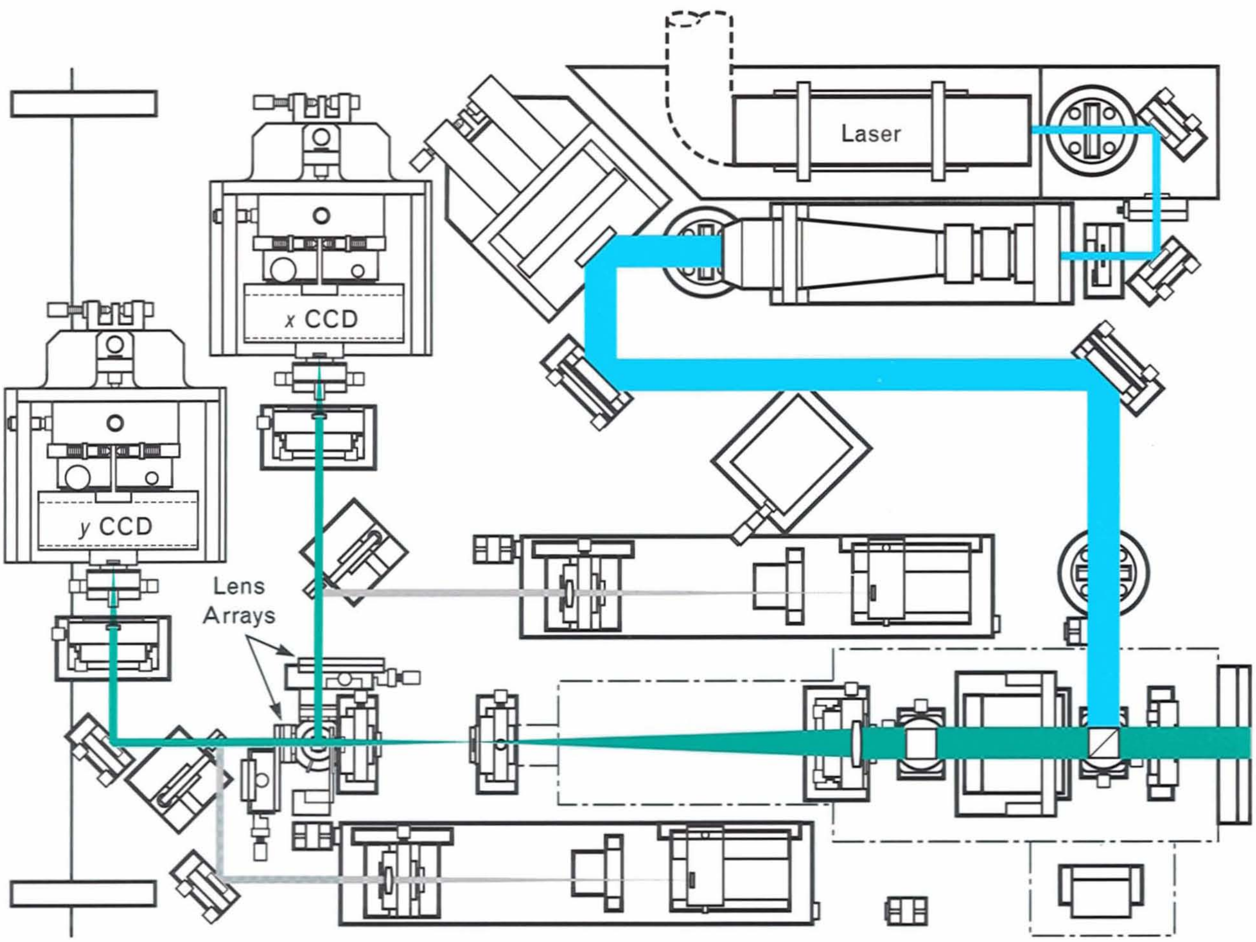


**FIGURE 9.** Optical layout of the wavefront sensor. The calibration beam, which is used to inject precisely known plane wavefronts into the sensor, is shown in blue. The external beam entering the sensor from the deformable mirror is shown in green. The Pockels cell and associated polarizers are used to shutter the light electronically on a sub-microsecond time scale. The gray path is used to perform alignment of the lens arrays with the deformable mirror actuators.

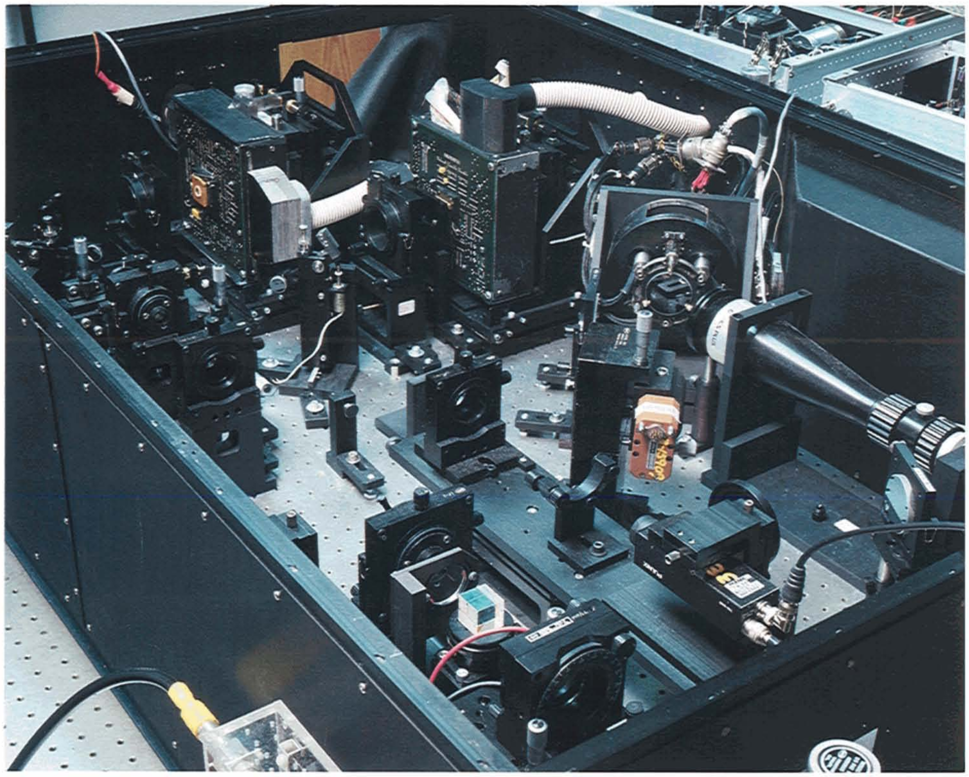

**FIGURE 10.** The SWAT wavefront sensor. Light enters the sensor from the bottom right edge of the photograph. The Pockels cell is the first visible component in the input beam path. The upper left portion of the sensor contains the lens arrays, which are hidden by their adjustable mounts. The CCD cameras and chips are visible in the back of the sensor. The CCD heads have individual cooling plenums, and air enters and exits via the flexible tubing. The flow of air reduces optical aberrations caused by heat sources in the sensor box.

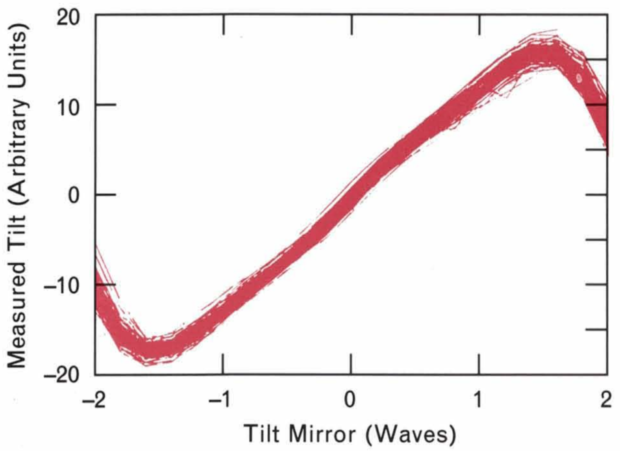


**FIGURE 11.** Measured transfer curves for all subapertures in the *x*-channel. The tilt reference mirror is scanned and the *x*-axis centroids are calculated for all subapertures. These data are the result of the uncorrected centroid calculation before tilt offset or gain adjustments have been made. The rms deviation of the slope from linear is $\lambda/29$.

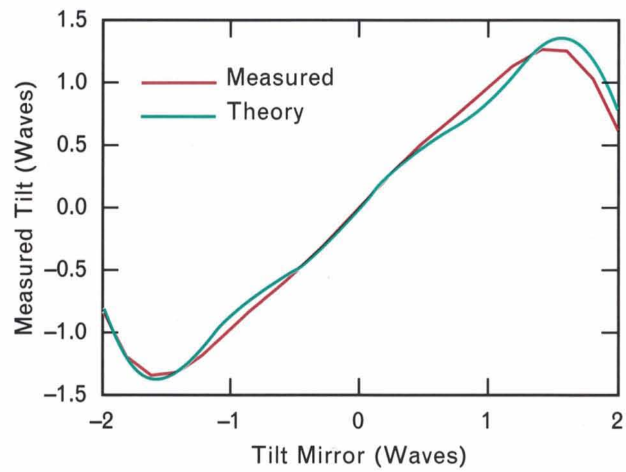


**FIGURE 12.** Comparison of the measured average transfer curve with theory. The transfer curve is more linear than expected, probably because of the soft edges of the CCD pixels. The theoretical calculation assumes sharp edges.

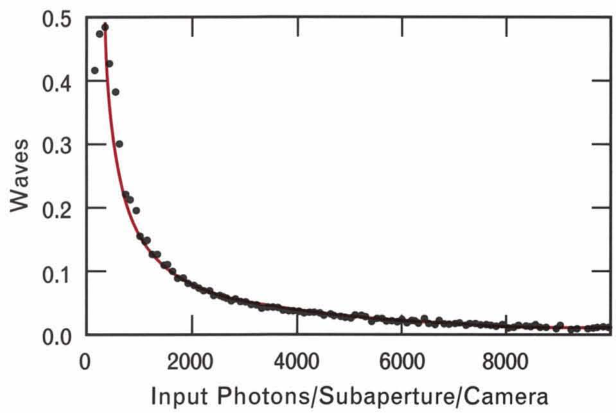


**FIGURE 13.** Predicted and measured temporal gradient noise as a function of incident subaperture light level for a wide range of illumination levels. The theoretical curve has only two free parameters—the quantum efficiency and the CCD noise floor—and measured values for these parameters were used.

Figure 13 compares the measured gradient noise with the theoretical noise performance. The gradient noise of the 4-pixel Hartmann sensor is [17]

$$\sigma^2 = \left(\frac{0.475}{GI_t^2}\right)\left(11.57n^2 + I_t\right),$$

where $\sigma^2$ is the tilt noise variance in rad$^2$ (at zero tilt), $G$ is the tilt gain (the slope of the transfer curve at zero tilt), $I_t$ is the total detected (corrected) intensity for the subaperture (expressed in number of electrons), and $n$ is the rms noise of the CCD camera (in number of electrons). This equation shows the dependence of the gradient noise on the incoming light level and camera readout noise. The sensor data are in excellent agreement with theory.

## Summary

A 241-channel Hartmann wavefront sensor was designed and built at Lincoln Laboratory for use in the SWAT atmospheric-compensation experiments. The sensor is capable of measuring wavefront gradients with an rms accuracy of $\lambda/15$ at 500 nm, at a light level of 2000 photons per subaperture. An entire frame of 16 × 16 gradients can be sensed, processed, reconstructed into phase, and used for accurately commanding the deformable mirror to a new figure, all within 300 $\mu$sec. The sensor can operate with either continuous or pulsed beacon radiation, and incorporates technologies that advance the state of the art in adaptive optics. These technologies include binary optics lens arrays, high-performance CCD focal-plane arrays and cameras, and a fast pipeline processor. The 64 × 64 CCD detectors have quantum efficiencies greater than 85% and 25 noise electrons at a readout rate of 7000 frames/sec. The architecture and software of the processing elements make the sensor robust and easy to use in a field environment.

## Acknowledgements

The authors gratefully acknowledge the microelectronics design group, particularly Ching-Ming Huang, Bob Mountain, Keith Percival, and Bob Holloway for both the device and the fabrication and testing of the camera electronics. Members of the binary optics group, particularly Phil Bundman, were essential in the fabrication of the lens arrays. The authors wish to acknowledge Charles Primmerman for his support and suggestions; Bob Carlson for the mechanical design; Irv Wigdor for the tilt calibration mirror; Frank Perry for providing the optical support; Dan Murphy and Byron Zollars for their suggestions and utilization of the sensor at the field site; and Walter Donnelly, Jai Gluckman, Paul Szarko, and Jim Tynan for assembling and testing the sensor electronics.

# REFERENCES

1. J.W. Hardy, J.E. Lefebvre, and C.L. Koliopoulos, "Real-Time Atmospheric Compensation," *J. Opt. Soc. Am.* **67**, 360 (1977).
2. D.P. Greenwood and C.A. Primmerman, "Adaptive Optics Research at Lincoln Laboratory," in this issue.
3. J. Herrmann, "Least-Squares Wavefront Errors of Minimum Norm," *J. Opt. Soc. Am.* **70**, 28 (1980).
4. R.J. Sasiela and J.G. Mooney, "An Optical Phase Reconstructor Based on Using a Multiplier-Accumulator Approach," *Proc. SPIE* **551**, 170 (1985).
5. C.A. Primmerman, D.V. Murphy, D.A. Page, B.G. Zollars, and H.T. Barclay, "Compensation of Atmospheric Optical Distortions Using a Synthetic Beacon," *Nature* **353**, 141 (12 Sept. 1991).
6. D.V. Murphy, "Atmospheric-Turbulence Compensation Experiments Using Cooperative Beacons," in this issue.
7. B.G. Zollars, "Atmospheric-Turbulence Compensation Experiments Using Synthetic Beacons," in this issue.
8. C.L. Koliopoulos, "Radial Grating Lateral Shear Heterodyne Interferometer," *Appl. Opt.* **19**, 1523 (1980).
9. D.L. Fried, "Limiting Resolution Looking Down through the Atmosphere," *J. Opt. Soc. Am.* **56**, 1380 (1966).
10. D.L. Fried, "Assessment of AOA Image Intensifier Noise Implications," *Technical Report* TR-764, The Optical Sciences Company (Nov. 1986).
11. R.R. Parenti, "Adaptive Optics for Astronomy," in this issue.
12. D.V. Murphy, C.A. Primmerman, B.G. Zollars, and H.T. Barclay, "Experimental Demonstration of Atmospheric Compensation Using Multiple Synthetic Beacons," *Opt. Lett.* **16**, 1797 (1991).
13. J.R. Leger, M. Holz, G.J. Swanson, and W.B. Veldkamp, "Coherent Laser Beam Addition: An Application of Binary-Optics Technology," *Lincoln Laboratory J.* **1**, 225 (1988).
14. J.C. Twichell, B.E. Burke, R.K. Reich, W.H. McGonagle, C.W. Huang, M.W. Bautz, J.P. Doty, G.R. Ricker, R.W. Mountain, and V.S. Dolat, "Advanced CCD Image Technology for Use from 1 to 10,000 A," *Rev. Sci. Instrum.* **61**, 2744 (1990).
15. C.M. Huang, B.E. Burke, B.B. Kosicki, R.W. Mountain, P.J. Daniels, D.C. Harrison, G.A. Lincoln, N. Usiak, M.A. Kaplan, and A.R. Forte, *Proc. 1989 International Symposium on VLSI Technology, Systems, and Applications, Taipei, Taiwan, May 1989,* p. 98.
16. R.K. Reich, R.W. Mountain, W.H. McGonagle, C.M. Huang, J.C. Twichell, B.B. Kosicki, and E.D. Savoye, "An Integrated Electronic Shutter for Back-Illuminated Charge-Coupled Devices," (International Electron Devices Meeting, Washington, Dec. 1991).
17. J.C. Twichell, "Hartmann Sensor Noise," Lincoln Laboratory Technical Report (in preparation).

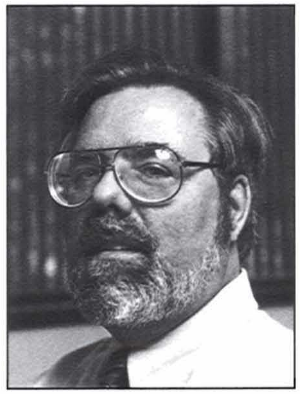

**HERBERT T. BARCLAY**
is an associate staff member in the High-Energy-Laser Beam Control and Propagation Group. His research is in atmospheric turbulence correction with adaptive optics. He received a B.A. in physics and an M.S.E.E. in electrooptics from Northeastern University. Before joining Lincoln Laboratory in 1985 he worked at the Frances Bitter National Magnet Laboratory at MIT.

**PHILLIP H. MALYAK**
is a staff member in the Advanced Techniques and Systems Group. He joined Lincoln Laboratory in 1985 and has worked on the design and analysis of optical systems for use in adaptive optics experiments. He is currently working in the area of infrared systems for discrimination. Phil received B.S. and M.S. degrees in electrical engineering from the State University of New York at Buffalo, and a Ph.D. degree in optics from the University of Rochester.

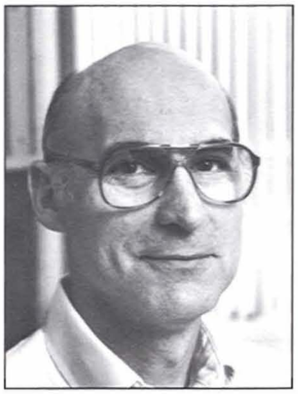

**WILLIAM H. MCGONAGLE**
is an associate staff member in the Microelectronics Group. His research is in analog and digital circuit design relating to CCD devices. He received a B.S.E.E. degree from Northeastern University, and he has been at Lincoln Laboratory for thirty years.

**ROBERT K. REICH**
is a staff member in the Microelectronics Group. His area of research is in the design of high-frame-rate and low-noise optical detector arrays. Bob received a B.S. degree from the Illinois Institute of Technology, and M.S. and Ph.D. degrees from Colorado State University, all in electrical engineering. He has been at Lincoln Laboratory since 1987, and he is a member of IEEE.

**GREGORY S. ROWE**
is an associate staff member in the High-Energy-Laser Beam Control and Propagation Group. His area of research is computer-aided instrumentation and control. Before joining Lincoln Laboratory in 1989, Greg worked at Ford Aerospace. He received a B.E. degree in electrical engineering and a B.S. degree in mathematics from Vanderbilt University.

**JONATHAN C. TWICHELL**
is a staff member in the High-Energy-Laser Beam Control and Propagation group. His research is in adaptive optics and detectors, and he has been at Lincoln Laboratory since 1985. He received an A.B. degree in physics from Earlham College, and M.S. and Ph.D. degrees in nuclear engineering from the University of Wisconsin at Madison.